Analysis of the Force on the Benzamide by Bubble Collapse Based on Molecular Dynamics Simulation

Wei XU*, Xiuli WANG, Jinhua LIU***, Yuanyuan ZHAO****, Guohui ZHAO*****,
Wenzhuo GUO********

**Research Center of Fluid Machinery Engineering and Technology, Jiangsu University, Zhenjiang, 212013, China,
E-mail: Xuwei791837@hotmail.com*
*** Research Center of Fluid Machinery Engineering and Technology, Jiangsu University, Zhenjiang, 212013, China;
Jiangsu Taifeng Pump Industry Co., Ltd, E-mail: ujslthb@163.com (Corresponding author)*
****International Shipping Research Institute, Gongqing Institute of Science and Technology, Jiujiang, 332020, China,
E-mail: liujinhua562@gmail.com*
*****School of the Environment and Safety Engineering, Jiangsu University, Zhenjiang, 212013, China,
E-mail: 1513876069@qq.com*
******Research Center of Fluid Machinery Engineering and Technology, Jiangsu University, Zhenjiang, 212013, China,
E-mail: 2212011044@stmail.ujs.edu.cn*
*******Research Center of Fluid Machinery Engineering and Technology, Jiangsu University, Zhenjiang, 212013,
China, E-mail: guowenzhuo@nuaa.edu.cn*

1. Introduction

It has been paid much attention and research since the cavitation is discovered in the early 20th century. In the present study, the dynamic properties of bubble induced by cavitation are closely related to the viscosity, surface tension and pressure of the liquid. Among them, the viscosity of liquid could delay the bubble collapse by slowing down the shrinkage rate of bubbles [1, 2]. However, bubble collapse accelerates with the increase of surface tension and pressure [3-5]. The interaction between the shock wave generated by bubble collapse and the wall is a hot topic. As for the study of bubble collapse, Adhikari et al. [6] used coarse particles to conduct molecular dynamics (MD) simulation in order to understand the mechanism of bubble collapse, and found that the pore size depended on both the velocity and the duration of the shock wave. Wu et al. [7] simulated the bubble collapse in the neural network and found that the local ultrasonic water hammer caused by the collapse of the asymmetric bubble would destroy hyaluronic acid. Zhou et al. [8] studied the bubble collapse to generate high-speed jet and shock waves, and found the shock wave reflected from the surface of molybdenum disulfide would enhance the spalling. Upendra et al. [9] studied the bubble collapse induced by shock wave, understood the detailed mechanism of cavitation induced damage to soft materials. Santo et al. [10] used the Martini coarser field to simulate the perforation of lipid bilayer caused by the collapse of nano-bubbles of different sizes, and summarized the formation of pores and damage rules of bilayer. Man et al. [11] induced the shock wave released by bubble collapse to penetrate the cell membrane and form small holes in the membrane by ultrasonic action, and found the shear stress generated by bubble vibration and the action mechanism of membrane holes. Ardeshir et al. [12] found that in the presence of nano-bubble, even if the shock wave pulse was relatively low, the collapse of bubble would cause serious damage to the model. Fu et al. [13] studied the collapse of bubble with different diame-

ters to calculate the force acting on the membrane, and revealed the relationship between impulse and bubble radius. Mahmud et al. [14] used MD simulation to study the pressure required for nanoscale cavitation growth in water and gel, and found that the time of bubble collapse was determined by the viscosity of the medium. Zhao et al. [15] studied the collapse characteristics of cylindrical holes by molecular dynamics, and summarized the evolution process of local pressure, temperature, pore size and shape during the collapse process. Then, Nan [16] and Vedadi et al. [17] adopted the same method, and found that the final shape of the bubble collapse was a ring structure, and the maximum volume of the cavitation area was related to the initial size of the bubble, and the length of the jet was linearly related to the radius of the bubble. Qiu et al. [18] studied the process of bubble collapse by analyzing the potential energy and motion of molecules, with emphasis on the influence of temperature on the dynamic characteristics of the bubble.

It is found from the above studies that there are few microscopic theoretical studies on cavitation degradation at present. The research on the dynamic process of bubble collapse is not clear, especially the research on the mechanism of the damage of pollutants caused by the shock wave and microjet caused by bubble collapse, which deserves attention. In the paper, the reactive force field (ReaxFF) is selected to calculate them, and the water molecular model is transferable interatomic potential with four-point model by the force balance method (TIP4P-FB) [19]. The research object is benzamide, and it is mainly used in the synthesis of medicines and dyes, and it is a toxic and carcinogenic dangerous product. It analyzes the influence of the initial bubble radius, the compressive strain rate and the temperature on the pressure release of bubble collapse on the pollutants, and it provides theoretical guidance for the application of cavitation and subsequent degradation of pollutants.

2. Model selections and simulation methods

2.1. Building models

In accordance with the structure information of benzamide molecules, the Materials Studio is used to generate the initial model of benzamide molecules, as shown in Fig. 1. Benzamide molecule consists of C, H, O, and N with a total of 16 atoms. Then, the Packmol program [20] is used to construct the initial position of the TIP4P-FB model. The water molecules and bubbles are distributed in the computational domain (60 Å x 60 Å x 60 Å), and the X, Y, and Z directions are set as periodic boundary conditions. The C language is used to add the upper and lower layers of the pollutants with a thickness of 5 Å in the Z direction of the computational domain, and the pollutants are composed of benzamide molecules. In the model, and the radii of the bubbles are 10, 12, and 15 Å, respectively. The distance between the bubbles and the upper wall of benzamide is 15 Å, while the distances from the lower wall of benzamide are 27, 33, and 37 Å, respectively.

Fig. 1 Benzamide molecule and Slice diagram of benzamide system

2.2. Force field selection

ReaxFF is a semiempirical interaction potential function based on the bond sequence first proposed by van Duin et al. [21] in 2001. It could effectively combine quantum chemistry and the molecular simulation method based on a nonreactive empirical force field, and aimed to provide a transferable potential energy to describe chemical reactions with bonding and fracture for accurately calculating chemical reaction energy and energy barrier. In this study, the ReaxFF is selected for simulation calculation.

ReaxFF generally contains 12 energy items [22]. The Eq. (1) can be expressed as:

$$E_{system} = E_{bond} + E_{lp} + E_{over} + E_{under} + E_{val} + E_{tor} + E_{coa} + E_{conj} + E_{H\text{-}bond} + E_{vdw} + E_{coul} + E_{pol}, \tag{1}$$

where: E_{bond}, E_{lp}, E_{over}, E_{under}, E_{val}, E_{tor}, E_{coa}, E_{conj}, $E_{H\text{-}bond}$, E_{vdw}, E_{coul}, and E_{pol} are the contributions of bond, lone pair, over-coordination, under-coordination, valence angle, torsion angle, three-body conjugate, four-body conjugate, hydrogen bond, van der Waals, Coulomb, and polarization energy, respectively.

2.3. Boundary condition

In simulation, the cutoff radius R_{cut} is set to 9.5 Å. The bond length and angle of TIP4P-FB water molecules are fixed by using the SHAKE algorithm. The initialization speed of the system satisfies the Maxwell–Boltzmann distribution and is randomly generated via the Maxwell distribution at the corresponding temperature. The Newton's integral equation of motion is solved numerically by using the velocity verlet algorithm. The Coulomb potential uses the particle–particle–particle–mesh method. The thermal bath coupling method is used to control temperature. The pressure could be calculated from the volume V, temperature T, and virial W. As shown in Eq. (2):

$$PV = Nk_B T + \frac{2}{3}\langle W \rangle. \tag{2}$$

The virial W is defined as:

$$W = \frac{1}{2}\sum_{j=1}^{N} \vec{r}_j \cdot \vec{F}_j. \tag{3}$$

The temperature T could be calculated from the instantaneous kinetic energy K.

$$T = \frac{2}{3Nk_B} K. \tag{4}$$

Substituting Eq. (3) and Eq. (4) into Eq. (2), it gets Eq. (5):

$$P = \frac{1}{V}\left(\sum_{j=1}^{N} m_j \vec{\upsilon}_j \vec{\upsilon}_j^{\,T} + \sum_{j=1}^{N} \vec{r}_j \vec{F}_j^{\,T}\right). \tag{5}$$

In Eq. (5), the right is Eq. (6) and Eq. (7):

$$\sum_{j=1}^{N} m_j \vec{\upsilon}_j \vec{\upsilon}_j^{\,T} = \begin{pmatrix} \sum_j m_j \upsilon_{jx}\upsilon_{jx} & \sum_j m_j \upsilon_{jx}\upsilon_{jy} & \sum_j m_j \upsilon_{jx}\upsilon_{jz} \\ \sum_j m_j \upsilon_{jy}\upsilon_{jx} & \sum_j m_j \upsilon_{jy}\upsilon_{jy} & \sum_j m_j \upsilon_{jy}\upsilon_{jz} \\ \sum_j m_j \upsilon_{jz}\upsilon_{jx} & \sum_j m_j \upsilon_{jz}\upsilon_{jy} & \sum_j m_j \upsilon_{jz}\upsilon_{jz} \end{pmatrix}. \tag{6}$$

$$\sum_{j=1}^{N} \vec{r}_j \vec{f}_j^{\,T} = \begin{pmatrix} \sum_j x_j F_{jx} & \sum_j x_j F_{jy} & \sum_j x_j F_{jz} \\ \sum_j y_j F_{jx} & \sum_j y_j F_{jy} & \sum_j y_j F_{jz} \\ \sum_j z_j F_{jx} & \sum_j z_j F_{jy} & \sum_j z_j F_{jz} \end{pmatrix}. \tag{7}$$

The instantaneous pressure tensor is calculated according to Eq. (5), and the instantaneous static pressure is 1/3 times the trace of the instantaneous pressure tensor:

$$P = \frac{1}{3}\left(P_{xx} + P_{yy} + P_{zz}\right). \tag{8}$$

Combined with Eq. (8) [23], the instantaneous static pressure released by bubble collapse could be obtained.

When performing MD calculations, the entire system with bubble radii of 10, 12, 15, and 20 Å should be relaxed. The system adopts a canonical ensemble, and the time step is set to 1 fs. After running 3000 steps, the system reaches the set temperature value and gradually stabilizes. After the relaxation, the temperature is 288, 298, and 308 K, the compressive strain rate is 0.0001, 0.0005, and 0.001, and the time step is set to 0.25 fs to run the entire system with 30,000 steps. The minus sign representing the direction about the compressive strain rate is omitted here. The data parameters of all molecules in the simulation area are obtained every 500 or 50 steps in accordance with the speed of bubble collapse. Lastly, the data obtained are analyzed and summarized.

3. Results and discussions

At present, in the microscopic aspect, scholars mainly study the characteristics of bubble collapse from temperature [18], viscosity [27], surface tension [26], cavitation nucleus [20], second phase particle size [24-25] to summarize its laws, but these researches on the force of bubble collapse on pollutant walls are not very in-depth. In this paper, it takes the pressure released from the upper and lower wall of benzamide by bubble collapse as the research object, and analyzes the influence of the initial radius of bubble, compressive strain rate and temperature on the pollutants.

3.1. Initial radius of bubbles

Three different sizes of bubble radii are 15, 12 and 10 Å in the model. The distance from the upper wall of benzamide is 15Å, and the distances from the lower wall of benzamide are 27, 33 and 37 Å, respectively. Fig. 2 is the variation rule of the pressure released on the upper and lower wall of benzamide with time when bubble collapses at compressive strain rate 0.0001 and temperature 298 K.

It can be seen from Fig. 2, a that the force on the upper wall of benzamide increases gradually and decreases rapidly when it reaches the maximum. At the same distance from the surface, the pressure of $R10$, $R12$ and $R15$ on the upper wall of benzamide is basically the same. When the bubble with radius of 10 Å collapses, the time to receive the maximum pressure on the upper wall of benzamide is longer than that of the other two radii. It can be also seen from Fig. 2, b, the force on the lower wall of benzamide increases gradually and decreases rapidly when it reaches the maximum. However, the bubble collapse of $R12$ receives the maximum pressure on the lower wall of benzamide. Comparing Fig. 2, a and 2, b, as the bubble radius increases, the released pressure first increases and then decreases. In order to explain the phenomenon well, assuming that the temperature of the liquid is a constant, the bubble is spherical, and

the radius of the bubble is R. The minimum energy W [28-29] required to form a bubble with a volume of V, and the value is the sum of the volume term W_1 and the surface term W_2.

a) Upper wall
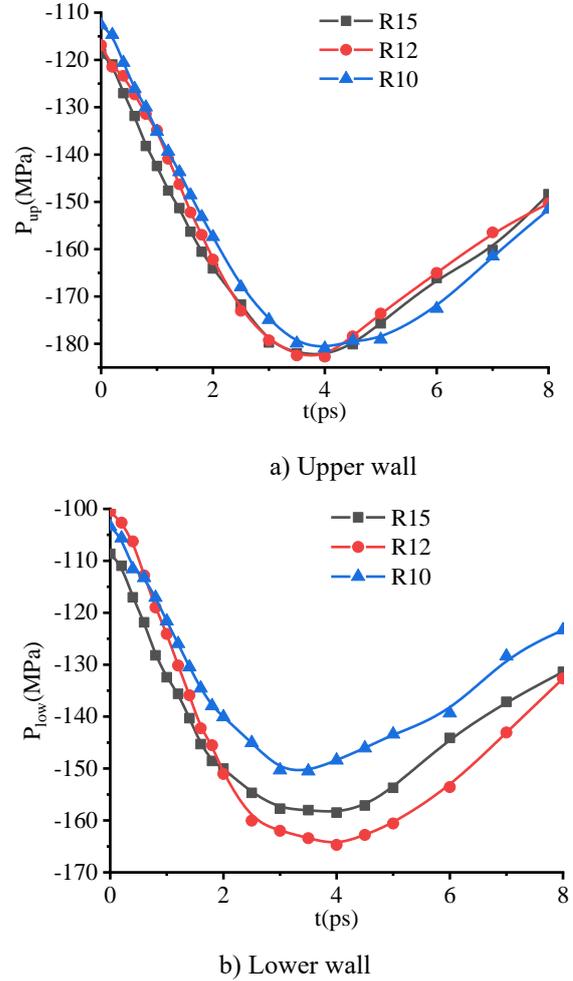
b) Lower wall

Fig. 2 Changes of pressure on the upper and lower wall of benzamide under different bubble radii

Assuming that the concept of surface tension is applicable to microscopic systems [30] and ignoring the influence of curvature, W can be obtained as:

$$W(R) = W_1 + W_2 = 4\pi R^2 \sigma_{LV} - \frac{4}{3}\pi R^3 (P_V - P_L). \tag{9}$$

In Eq. (9), P_V is the gas pressure, and P_L is the liquid pressure. σ_{LV} is the surface tension of vapor and liquid, and A is the surface area of the bubble. When the fluid and temperature are given, the energy first increases and then decreases from Eq. (11) with the increase of the bubble radius.

Fig. 3 shows that the relationship between the maximum force on the upper and lower wall of benzamide and the radius of the bubble in the process of bubble collapse. It can be seen from Fig. 3 that, with the increase of bubble radius, the maximum pressure on the upper and lower wall of benzamide first increases, then decreases, and then tends to remain constant. However, the impact of bubble collapse on the upper wall is greater than that on the lower wall, which may be related to the fact that the bubble is closer to the

upper wall and farther to the lower wall. With the increase of the bubble radius, the difference between the maximum pressure on the upper and lower wall of benzamide increases gradually, and then has a constant trend. In Fig. 3, when it is used to release energy to treat pollutants or the metal wall by bubble collapse, the recommended bubble radius is 10-15 Å, and the energy released at this time is the most.
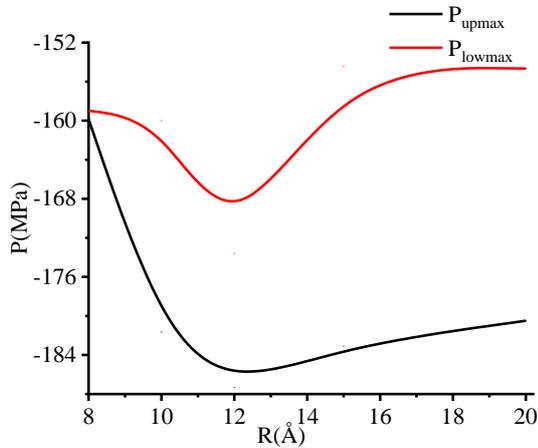
Fig. 3 Maximum pressure on the upper and lower wall of benzamide varies with the bubble radius

3.2. Compressive strain rate

Fig. 4 shows the variation of pressure released on the upper and lower wall of benzamide with time at different
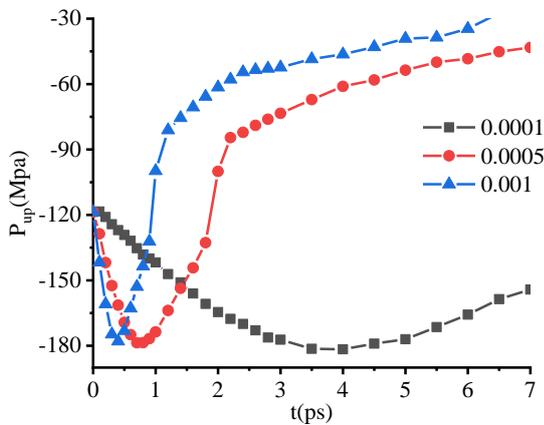
a) Upper wall
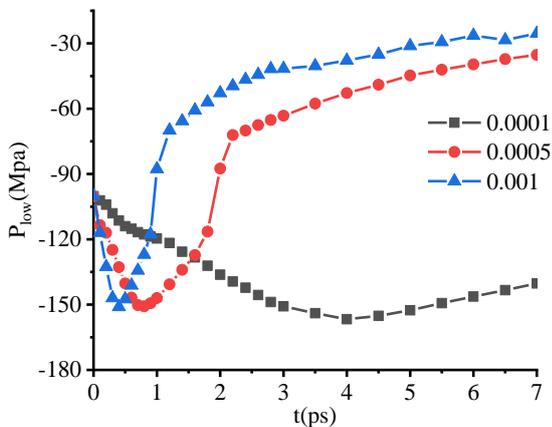
b) Lower wall

Fig. 4 Changes of pressure on the upper and lower wall of benzamide at different compressive strain rates

compressive strain rates when the bubble radius is 15 Å and the temperature is 298 K.

It can be seen from Fig. 4, a that when the temperature is 298 K and the radius is 15 Å, the pressure on the upper wall of benzamide increases rapidly with time at the same compressive strain rate. When it reaches the maximum value, it decreases rapidly and then slowly. With the increase of compressive strain rate, the time for the upper wall of benzamide to be subjected to the maximum pressure is gradually shortened, indicating that compressive strain rate has a great influence on the rate of pressure release of bubble, and it has a great influence on the collapse time. It can be seen from Fig. 4, b that when the temperature is 298 K and the radius is 15 Å, the pressure on the lower wall of benzamide increases rapidly with time at the same compressive strain rate. When it reaches the maximum value, it decreases rapidly and then slowly. With the increase of the compressive strain rate, the time for the lower wall of benzamide to be subjected to the maximum pressure gradually decreases, indicating that the compressive strain rate has a great influence on the rate of pressure release of the bubble and has a great influence on the collapse time. It can be seen from the figures that the law of stress on the upper and lower wall of benzamide is consistent, and the time of maximum pressure on the upper and lower wall of benzamide is consistent. When the temperature is 298 K and the radius is 15 Å, the maximum pressure on the upper wall of benzamide is greater than the maximum pressure on the lower wall from Fig. 5.
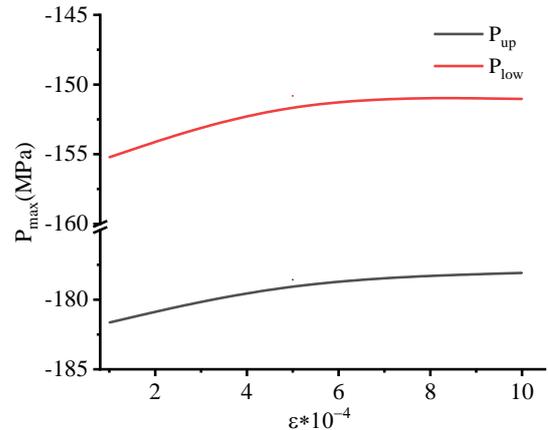
Fig. 5 Maximum pressure on the upper and lower wall of benzamide varies with the compressive strain rate

In Fig. 5, with the increase of compressive strain rate, the maximum pressure released by bubble collapse gradually decreases and then tends to be constant. The maximum pressure difference between the upper wall and the lower wall of benzamide does not change with the increase of compressive strain rate. Under each compressive strain rate, the sum of the maximum pressure between the upper and the lower wall of benzamide is basically the same, in line with the principle of energy conservation.

3.3. Temperature

Fig. 6 shows the change rule of the pressure released on the upper and lower wall of benzamide with time at different temperatures when the bubble radius is 15 Å and the compressive strain rate is 0.0001.

It can be seen from Fig. 6a that when the compressive strain rate is 0.0001 and the radius is 15 Å, the pressure on the upper wall of benzamide increases rapidly with time at the same temperature, and then decreases rapidly when it reaches the maximum value. With the increase of temperature, the time of maximum pressure on the upper wall of benzamide is basically the same. It can be seen from Fig. 6, b that the pressure on the lower wall of benzamide increases rapidly with time at the same temperature, and then decreases rapidly when it reaches the maximum value. With the increase of temperature, the maximum pressure on the lower wall of benzamide increases first and then tends to be constant. The rate of pressure release by bubble collapse is basically the same, indicating that the collapse time is basically not affected within this temperature range from Figs. 6, a and 6, b.

a) Upper wall
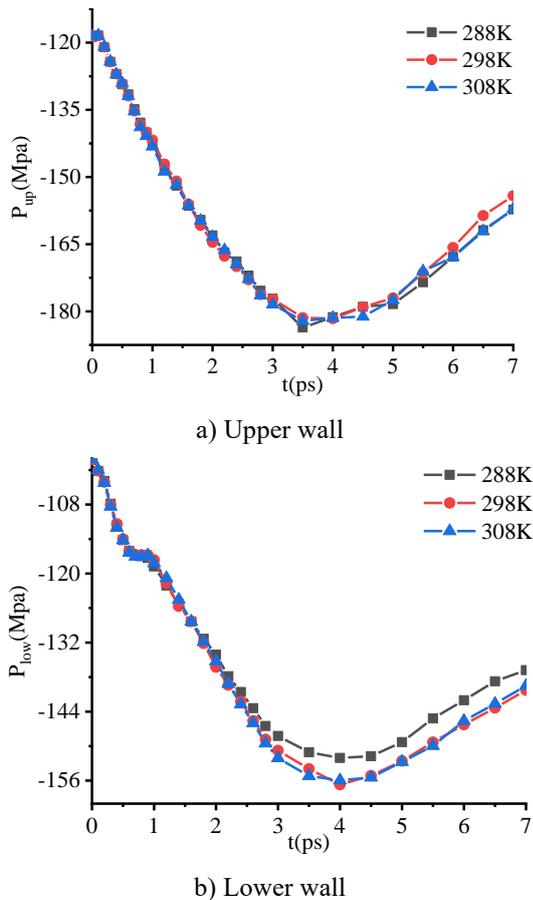
b) Lower wall

Fig. 6 Changes of pressure on the upper and lower wall of benzamide at different temperatures

Fig. 7 shows that the relationship between the maximum force on the upper and lower wall of benzamide and the temperature in the process of bubble collapse.

It can be seen from Fig. 7 that when the compressive strain rate is 0.0001 and the radius is 15 Å, the maximum pressure on the upper wall of benzamide is greater than that on the lower wall. With the increase of temperature, the maximum pressure released by bubble collapse on the upper wall of benzamide decreases gradually, and then tends to be constant. The maximum pressure released by bubble collapse on the lower wall of benzamide increases gradually and then tends to be constant. At the same temperature, the maximum pressure difference between the upper and the

lower wall of benzamide decreases with the increase of temperature, and then tends to be constant. And at each temperature, the sum of the maximum pressure between the upper and lower wall of benzamide is basically the same, in line with the principle of energy conservation.
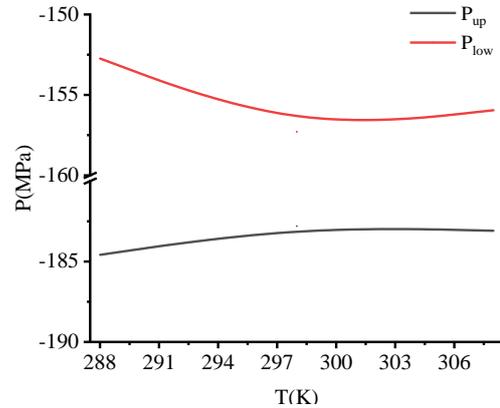
Fig. 7 Maximum pressure on the upper and lower wall of benzamide varies with the temperature

3.4. Analysis of the relationship of various factors on benzamide wall

It can be seen from Figs. 2, 4 and 6 that compressive strain rate 0.0001, bubble radius 15 Å and temperature 298 K are included in each factor analysis. Therefore, this level of each factor is taken as the benchmark and the pressure and collapse time on the upper and lower wall of benzamide are taken as the targets to compare the primary and

a) Upper wall
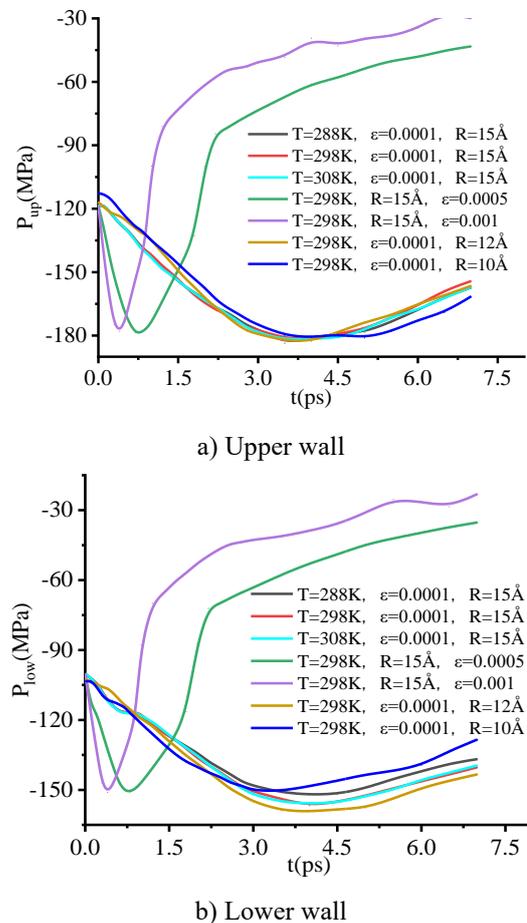
b) Lower wall

Fig. 8 Changes of pressure on the upper and lower wall of benzamide with time under different factors

secondary relationships of the three factors, as shown in Fig. 8.

As can be seen from Fig. 8, the temperature, compressive strain rate and bubble radius have an impact on the collapse time of bubble. Based on the speed of bubble collapse, the compressive strain rate has a great influence, while the temperature and the size of the bubble radius have little influence.

To further study the effect of bubble collapse, based on the force of bubble collapse on the pollutants, the maximum pressure on the upper and lower wall of benzamide when the initial bubble radius of 15 Å collapses is calculated as shown in the Table. 1.

According to Fig. 8 and Table 1, bubble radius, compressive strain rate and temperature affect the pressure on the upper and lower wall of benzamide. Based on the pressure released by bubble collapse on the benzamide wall, the analysis and comparison show that the influence of bubble radius and temperature is large, and the influence degree of the two factors is roughly the same, while the influence of compressive strain rate is small.

Table 1

The maximum pressure on the benzamide wall under different compressive strain rates and temperatures

Maximum pressure, MPa	Compressive strain rate, 10^{-4}			Temperature, K		
	1	5	10	288	298	308
Upper wall	182.8	178.7	178.1	184.5	182.8	183.1
Lower wall	157.2	150.8	150.5	152.7	157.2	155.7

4. Conclusions

In this paper, it establishes benzamide models containing bubbles with different radii, and reveals the influence of the initial radius, compressive strain rate and temperature on the release pressure of bubble collapse on the pollutants. The conclusions are summarized as follows:

1. As the initial radius of the bubble increases, the maximum pressure on the upper and lower wall of the benzamide increases first, then decreases, and then tends to remain unchanged.

2. The maximum pressure difference between the upper and the lower wall of benzamide does not change with the increase of the compressive strain rate.

3. With the increase of temperature, the maximum pressure on the upper and lower wall of the benzamide both increase first, and then tend to remain unchanged.

4. Based on the pressure on the upper and lower wall of the benzamide, the temperature and the initial radius of the bubble have a large influence, and the influence of the compressive strain rate is small.

At present, how to choose the force field, the medium system, and the model material accurately and construct the gas core close to the real water is essential. Most of the existing studies have conducted qualitative analysis on the characteristics that affect bubble collapse. Many challenges remain in the quantitative study of the influencing factors of bubble collapse. In the future research, the MD simulation results should be further analyzed combined with experiments.

References

1. **Aghdam, A. Hajizadeh.; Ohl, S. W.; Khoo, B. C.;** et al. 2012. Effect of the viscosity on the behavior of a single bubble near a membrane, International Journal of Multiphase Flow 47(3): 17-24.
https://doi.org/10.1016/j.ijmultiphaseflow.2012.06.010.

2. **Lu, M.; Ning, Z.; Yan, K.;** et al. 2014. Breakup of cavitation bubbles within the diesel droplet, Chinese Journal of Mechanical Engineering 27(1): 198-204.
https://doi.org/10.3901/CJME.2014.01.198.

3. **Samiei, E.; Shams, M.; Ebrahimi, R.** 2011. A novel numerical scheme for the investigation of surface tension effects on growth and collapse stages of cavitation bubbles, European Journal of Mechanics B/Fluids 30: 41-50.
https://doi.org/10.1016/j.euromechflu.2010.09.002.

4. **Brouwer, G. C.; Wagner, E. C.; Van Ommen, J. R.;** et al. 2012. Effects of pressure and fines content on bubble diameter in a fluidized bed studied using fast X-ray tomography, Chemical Engineering Journal 207: 711-717.
https://doi.org/10.1016/j.cej.2012.07.040.

5. **Li, B. B.; Zhang, H. C.; Lu, J.;** et al. 2011. Experimental investigation of the effect of ambient pressure on laser-induced bubble dynamics, Optics & Laser Technology 43: 1499-1503.
https://doi.org/10.1016/j.optlastec.2011.05.016.

6. **Adhikari, U.; Goliaei, A.; Berkowitz, M. L.** 2015. Mechanism of membrane poration by shock wave induced nanobubble collapse: a molecular dynamics study, The Journal of Physical Chemistry B 119: 6225-6234.
https://doi.org/10.1021/acs.jpcb.5b02218.

7. **Wu, Y. T.; Adnan, A.** 2017. Effect of shock-induced cavitation bubble collapse on the damage in the simulated perineuronal net of the brain, Scientific Reports 7(1).
https://doi.org/10.1038/s41598-017-05790-3.

8. **Zhou, G. Q.; Rajak, P.; Susarla, S.;** et al. 2018. Molecular Simulation of MoS2 Exfoliation, Scientific Reports 8.
https://doi.org/10.1038/s41598-018-35008-z.

9. **Adhikari, U; Goliaei, A; Berkowitz, M. L.** 2016. Nanobubbles, cavitation, shock waves and traumatic brain injury, Royal Society of Chemistry 18(48): 32638-32652.
https://doi.org/10.1039/c6cp06704b.

10. **Santo, K. P.; Berkowitz, M. L.** 2014. Shock wave interaction with a phospholipid membrane: Coarse-grained computer simulations, The Journal of Chemical Physics 140.
https://doi.org/10.1063/1.4862987.

11. **Man, V. H.; Truong, P. M.; Li, M. S.;** et al. 2019. Molecular mechanism of the cell membrane pore formation induced by bubble stable cavitation, The Journal of Physical Chemistry B 123: 71-78.
https://doi.org/10.1021/acs.jpcb.8b09391.

12. **Goliaei, A.; Adhikari, U.; Berkowitz, M. L.** 2015. Opening of the blood-brain barrier tight junction due to shock wave induced bubble collapse: a molecular dynamics simulation study, ACS Chemical Neuroscience 6(8): 1296-1301.
https://doi.org/10.1021/acschemneuro.5b00116.

13. **Fu, H. H.; Comer, J.; Cai, W. S.;** et al. 2015. Sonoporation at small and large length scales: effect of cavitation bubble collapse on membranes, The Journal of Physical Chemistry Letters 6: 413-418.
https://doi.org/10.1021/jz502513w.

14. **Al Mahmud, K. A. H.; Hasan, F.; Khan, M. I.;** et al. 2020. On the molecular level cavitation in soft gelatin hydrogel, Scientific Reports 10(1).
https://doi.org/10.1038/s41598-020-66591-9.

15. **Zhao, P. H.; Lee, S. Y.; Sewell, T.;** et al. 2020. Tandem Molecular Dynamics and Continuum Studies of Shock-Induced Pore Collapse in TATB, Propellants Explosives Pyrotechnics 45(2):196-222.
https://doi.org/10.1002/prep.201900382.

16. **Nan, N.; Si, D.Q.; Hu, G. H.** 2018. Nanoscale cavitation in perforation of cellular membrane by shock-wave induced nanobubble collapse, The Journal of Chemical Physics 149.
https://doi.org/10.1063/1.5037643.

17. **Vedadi, M.; Choubey, A.; Nomura, K.;** et al. 2010. Structure and dynamics of shock-induced nanobubble collapse in water, Physical Review Letters 105.
https://doi.org/10.1103/PhysRevLett.105.014503.

18. **Qiu, C.; Chen, H.; Zhou, C. C.** 2018. Molecular dynamics simulation on cavitation bubble collapse, Mechanika 24(1): 56-60.
https://doi.org/10.5755/j01.mech.24.1.15127.

19. **Wang, L. P.; Martinez, T. J.; Pande, V. S.** 2014. Building force fields: an automatic, systematic, and reproducible approach, The Journal of Physical Chemistry Letters 5(11): 1885-1891.
https://doi.org/10.1021/jz500737m.

20. **Martínez, L.; Andrade, R.; Birgin, E. G.;** et al. 2009. PACKMOL: a package for building initial configurations for molecular dynamics simulations, Journal of Computational Chemistry 30(13): 2157-2164.
https://doi.org/10.1002/jcc.21224.

21. **Van Duin, A. C. T.; Dasgupta, S.; Lorant, F.;** et al. 2001. ReaxFF: a reactive force field for hydrocarbons, The Journal of Physical Chemistry A 105(41): 9396-9409. https://doi.org/10.1021/jp004368u.

22. **Xu, W.; Zhu, R.S.; Wang, J.;** et al. 2022. Molecular dynamics simulations of the distance between the cavitation bubble and benzamide wall impacting collapse characteristics, Journal of Cleaner Production 352: 131633.
https://doi.org/10.1016/j.jclepro.2022.131633.

23. **Chen, Z. L.; Xu, W. R.; Tang, L. D.;** et al. 2007. The theory and practice of molecular simulation, Chemical Industry Press 108-110.

24. **Gu, Y. W.; Li, B. X.; Chen, M.** 2016. An experimental study on the cavitation of water with effects of SiO_2 nanoparticles, Experimental Thermal and Fluid Science 79: 195–201.
https://doi.org/10.1016/j.expthermflusci.2016.07.009.

25. **Jackson, S.; Nakano, A.; Vashishta, P.;** et al. 2019. Electrostrictive cavitation in water induced by a SnO_2 nanoparticle, ACS omega 4: 22274−22279.
https://doi.org/10.1021/acsomega.9b00979.

26. **Wu, W. D.; Shao, J. L.** 2020. Atomistic study on the dynamic response of the void or helium bubble in aluminum under compression and tension, Journal of Applied Physics 127: 154902.
https://doi.org/10.1063/5.0004698.

27. **Gregersen, S. B.; Wiking, L.; Bertelsen, K. B.;** et al. 2019. Viscosity reduction in concentrated protein solutions by hydrodynamic cavitation, International Dairy Journal 97: 1-4.
https://doi.org/10.1016/j.idairyj.2019.04.015.

28. **Fisher J. C.** 1948. The Fracture of Liquids, Journal of Applied Physics 19(11): 1062-1067.

29. **Blander, M.; Katz, J. L.** 1975. Bubble nucleation in liquids, AIChE Journal 21(5): 833-848.

30. **Mikhail, P.; Anisimov.** 2003. Nucleation: theory and experiment, Russian Chemical Reviews 72(7).

W. Xu, X. L. Wang, J. H. Liu, Y. Y. Zhao, G. H. Zhao, W. Z. Guo

ANALYSIS OF THE FORCE ON THE BENZAMIDE BY BUBBLE COLLAPSE BASED ON MOLECULAR DYNAMICS SIMULATION

S u m m a r y

The cavitation damage of the pollutant wall caused by shock wave and microjet in the process of bubble collapse has attracted widespread attention. However, many researches focus on bubble collapse from the macroscopic experimental point of view, the dynamics of which is still not clear. In this paper, it takes the pressure on the upper and lower wall of pollutants as the research target, and summarizes the influence of initial radius of bubbles, compressive strain rates and temperatures on the release pressure of bubble collapse on the pollutants. The results show that: as the initial radius of bubbles increase, the maximum pressure on the upper and lower wall of benzamide increases first and then decreases. The pressure release rate of bubble increases with the increase of the compressive strain rate. Based on the pressure on the upper and lower wall of the benzamide, the temperature and initial radius of the bubble have a large influence, and the influence of the compressive strain rate is small. The paper provides theoretical guidance for the application of cavitation.

Key words: MD simulation, bubble collapse, benzamide model, factor parameters, wall forces.